JMI Journal of Medical Imaging

RESEARCH PAPER

Analysis of DWT–DCT watermarking algorithm on digital medical imaging

Rajkumar Soundrapandiyan, Kannadasan Rajendiran, Arunkumar Gurunathan, Akila Victor, and Ramani Selvanambi*

Vellore Institute of Technology, School of Computer Science and Engineering, Vellore, Tamil Nadu, India

ABSTRACT. **Purpose:** Over the past decade, the diagnostic information of the patients are digitally recorded and transferred. During the transmission of patients data, the security and authenticity of the information has to be ensured. Medical image watermarking technology has recently advanced because it can be used to conceal patient information while ensuring the authenticity. We propose a multiple watermarking method for securing clinical medical images.

Approach: In this watermarking method, the quality feature property and private label property information are embedded as watermarks in the original image. Initially, medical images are divided into the region of interest (ROI) and non-interest region (NIR). Second, a two-level discrete wavelet transform (DWT) is applied to the ROI and the coefficients LL1 (LL2, LH2, HL2, HH2), LH1, HL1, and HH1 are generated. Watermarks are embedded using the DWT low-frequency sub-band (LL2) by quantizing the low-frequency coefficients. Next, the NIR is separated into non-overlapping 8×8 blocks, and a discrete cosine transform (DCT) is applied for each block. The DCT coefficients of each block are sorted using the zigzag transform. For embedding, eight intermediate frequency coefficients are used. Finally, the feature information is embedded in the ROI, and the tag information is embedded in the NIR.

Results: The performance of the DWT-DCT watermarking method is calculated using the metrics of peak signal-to-noise ratio (PSNR), structural similarity index measure, and mean square error. The proposed method obtained the better PSNR value of 45.76 dB.

Conclusions: The proposed model works well for clinical medical images when compared with the existing techniques.

Keywords: medical image; multiple watermarks; quantization; region of interest; non-interest region; discrete wavelet transform; discrete cosine transform; zigzag sort; Arnold transform; logistic encryption; peak signal-to-noise ratio; structural similarity index measure; mean square error

Paper 22364GRR received Dec. 24, 2022; revised Nov. 16, 2023; accepted Dec. 11, 2023; published Dec. 28, 2023.

1 Introduction

Since the advent of the Internet, a new field known as telemedicine has emerged; it has made access to healthcare and accessibility of records easier. Hospitals in many countries use electronic patient records to maintain patients' medical data (diseases name, disease size, disease affected area, etc.), private data (name, birth date, gender, address, etc.), and financial data (payment by

*Address all correspondence to Ramani Selvanambi, ramani.s@vit.ac.in

2329-4302/2023/$28.00 © 2023 SPIE

cash/debit card/credit card/UPI), and these can be transferred to any corner of the world with accessibility to the Internet.[1] But the data may get tampered with unintentionally or intentionally while being transferred. To prevent a misdiagnosis, sensitive, private, and useful information can be encrypted and embedded into it in the form of a watermark. This would serve as a medium not only of authentication but also of integrity.[2,3] In recent years, a significant amount of work has been carried out for watermarking algorithms in medical images.

In 2004, Nayak et al.[4] developed a watermarking algorithm with embedding and encryption techniques. In 2006, Trichili et al.[5] presented the watermarking embedding algorithm with encryption and decryption methods to secure the patient information. In 2007, Zian et al.[6] introduced the reversible watermarking approach for embedding the secure patient information. In 2011, Osamah et al.[7] used the fragile watermarking technique to embed the patient's information in the transform domain. In 2010, Salwa et al.[8] developed the watermarking algorithm using a wavelet based data embedding approach. In 2015, Lu et al.[1] proposed the multiple watermarking scheme that used the discrete wavelet transform (DWT) and discrete cosine transform (DCT) techniques. In 2017, Natu et al.[9] combined singular vector decomposition (SVD) and DCT to embed the patient information in the cover image. In 2018, Assini et al.[10] proposed a watermarking method by combining the DWT, DCT, and SVD. In 2020, Begum et al.[11] developed a watermarking method in the hybrid domain. In the hybrid domain watermarking scheme, many methods, such as DCT+DWT, DCT+DWT, DCT+SVD, DFT+DWT, DFT+SVD, DCT+DFT+DWT, have been introduced. The summary of the existing watermarking techniques, evaluations metrics, and limitation are shown in Table 1.

From the literature and Table 1, it can be seen that many of the works suffer from a lower payload capacity and less robustness and takes more computational time. This drawback motivated us to develop a new watermarking method. In this paper, a new watermarking algorithm using multiple watermarks for computed tomography (CT) medical images is presented. In this

Table 1 Summary of the existing watermarking techniques.

Ref no.	Methodology	Metrics	Limitation
4	Embedding using encryption methods (hamming code, Bose–Chaudhuri–Hocquenghem codes)	• PSNR	Fails to retrieve the hidden information properly
5	Binary coding technique, asymmetric based encryption and decryption method	• PSNR • MSE	The method is not robust against some attacks
6	ROI and RONI extraction method and LSB method for embedding	• PSNR • SSIM	The method fails to get back 100% of watermark patient information
7	Fragile watermarking achieved using transform domain and neural network	• PSNR • MAE	Due to neural network and transform domain, is time consuming.
8	Wavelet transformation for embedding	• PSNR • SSIM	Wavelet domain is time consuming.
1	DWT and DCT	• PSNR • SSIM	ROI detected manually
9	Single vector decomposition and DCT	• PSNR • SSIM • MAE	The process of embedding is time consuming due to SVD decomposition
10	DWT, single vector decomposition, DCT	• PSNR • NCC • SSIM	The method fails in the reversal process
11	Hybrid method (DCT+DWT, DCT+DWT, DCT+SVD, DFT+DWT, DFT+SVD, DCT+DFT+DWT)	• PSNR • BER • MAE • NCC	Time consuming but robust against common attacks

method, initially, the whole medical image is divided into the region of interest (ROI) and non-interest region (NIR). Next, the image key feature information is embedded in the ROI with the help of DWT. Then, private label property tag information is embedded in NIR using the DCT. Before embedding, both ROI and NIR watermarks are encrypted using logistic map encryption and Arnold transform, respectively.

The remainder of this paper is organized as follows: Sec. 2 presents the methodologies used to propose the new watermarking method. Sec. 3 presents the proposed method, Sec. 4 presents the experimental results and performance analysis, and Sec. 5 concludes this paper.

2 Materials and Methods

2.1 Discrete Wavelet Transform

DWT is one of the basic wavelet transforms in which wavelets are sampled discretely. A fundamental benefit of DWT is temporal resolution, and it captures both frequency and location details. Hence, in this paper, DWT is used. The DWT gets the low frequency and high frequency subbands of image by applying L-level of DWT on the ROI of the original image. After the L-level of DWT, on the low frequency subband, image watermark information is embedded because, in this location, the image can have improved imperceptibility. The DWT characteristic is used to identify tampering in medical images. The DWT is defined in Eqs. (1) and (2):

$$F_{\varphi}(i_0,a,b)=\frac{1}{\sqrt{AB}}\sum_{a=0}^{A-1}\sum_{b=0}^{B-1}f(a,b)\varphi_{i_0,a,b}(a,b), \tag{1}$$

$$F_{\psi}(i_0,a,b)=\frac{1}{\sqrt{AB}}\sum_{a=0}^{A-1}\sum_{b=0}^{B-1}f(a,b)\psi^{j}_{i_o,a,b}(a,b)\quad i=\{LH,HL,HH\}, \tag{2}$$

where $f(a,b)$ is the original image; A and B are the number of row and column of the image, respectively; $F_{\Phi}(i_o,a,b)$ is the low frequency subband; and $F_{\Psi}(i_o,a,b)$ is the high frequency subband.

2.2 Logistic System

The digital watermark information from the watermarked images can be extracted by any person in the public during transmission/usage. This may lead to the tampering of the watermarked image, which creates several problems. So, before embedding, the digital watermark information in the medical image is encrypted.

In this paper, a logistic map mechanism is used for the encryption. The mathematical expression of the logistic map is given as

$$T_{m+1}=\mu T_m(1-T_m),\quad \mu\in[0,4],\quad T\in[0,1], \tag{3}$$

where μ is a logistic map parameter. The logistic map is in a chaotic state when $T\in[0,1]$. The value of the μ sequence is iteratively generated.

2.3 Arnold Transform

To improve the security of the watermarking process, Arnold transform is used. Basically, Arnold transform scrambles the pixels, and it makes the decryption process complex. A two-dimensional (2-D) Arnold transform is given as

$$\begin{bmatrix}P'\\Q'\end{bmatrix}=\begin{bmatrix}1&1\\1&2\end{bmatrix}\begin{bmatrix}P\\Q\end{bmatrix}\bmod W, \tag{4}$$

where P and Q are the coordinates pixel of the image, W is the width of the image, and P' and Q' are the coordinates of the scrambled image.

2.4 DCT

The DCT function expresses the sequence of data points into the sum of cosine functions. DCT is the energy compaction property. DCT provides good results on the signal processing and image processing applications. The 2-D DCT function is defined as

$$T(i,j) = \alpha(i)\alpha(j)\sum_{a=0}^{N-1}\sum_{b=0}^{N-1} t(a,b)\cos\frac{(2a+1)\pi i}{2N}\cos\frac{(2b+1)\pi j}{2N}. \quad (5)$$

The inverse 2-D DCT function is defined as

$$t(a,b) = \alpha(i)\alpha(j)\sum_{i=0}^{N-1}\sum_{j=0}^{N-1} T(i,j)\cos\frac{(2a+1)\pi i}{2N}\cos\frac{(2b+1)\pi j}{2N}, \quad (6)$$

where $T\ (i,j)$ is the DCT coefficient of function $t(a,b)$.

The DCT coefficients of the non-overlapping 8×8 blocks are divided into three bands, the low frequency band, middle frequency band, and high frequency band, and only the middle frequencies of the zigzag sort are used. The patient tag information is embedded in the NIR using a block-wise DCT transform along with a zigzag sort of each block.

3 Proposed System Design

The proposed system is implemented in four stages:

- ROI generation and ROI watermark generation;
- NIR generation and NIR watermark generation;
- Embedding process;
- Extraction process.

3.1 ROI Generation and ROI Watermark Generation

3.1.1 *ROI generation*

ROI generation is one of the important processes for digital watermarking. To generate the ROI, the popular iterative thresholding algorithm is used in this paper. The iterative thresholding technique is used to select the optimal threshold value for binarization of the medical image. Next, on the binarization medical image, the binary mask is applied iteratively to clean out any erroneous areas, as shown in Fig. 1. The cleaned binarization medical image is then used to generate the regions from the original medical image.

3.1.2 *ROI watermark generation*

Basically, medical images show the growth of human organs. These organs are always fixed size and shape. So, the area, solidity, eccentricity, area ratio, and perimeter of the ROI are used as the watermark information. Figure 2 shows the ROI watermark, which is generated from the ROI.

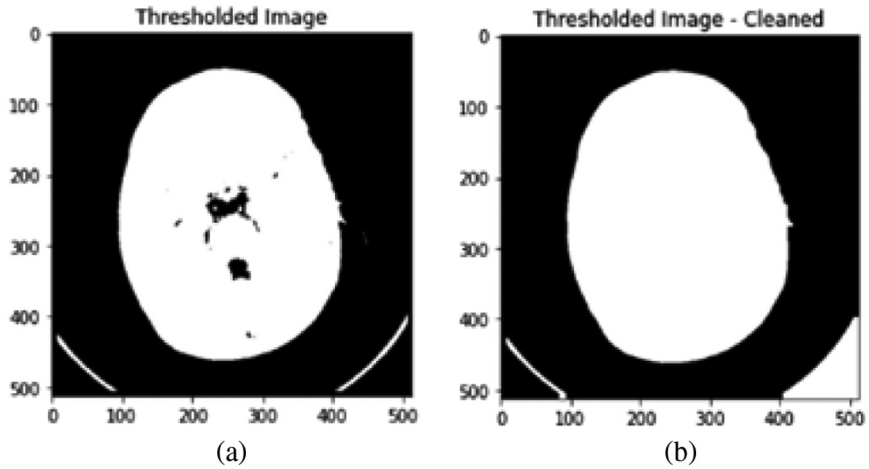

Fig. 1 (a) Binarization of medical image using iterative thresholding and (b) cleaned binarization medical image.

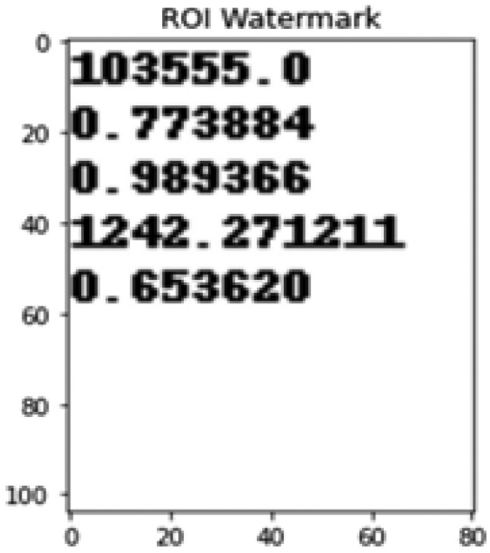

Fig. 2 ROI watermark.

3.2 NIR Generation and NIR Watermark Generation

3.2.1 *NIR generation*

After the selection of the ROI, the remaining region from the original image is considered to be the NIR region. The size of the NIR region is evaluated because embedding of the watermarking information in the DCT domain should be the block of 8×8. Hence, the NIR region is repeatedly evaluated, until the boundary is divisible by 8.

3.2.2 *NIR watermark generation*

The patient information along with the institute logo is used as the NIR watermark information. For the implementation, we use a standard tag information watermark of 64×64 in size. Figure 3 shows the NIR watermark information.

3.3 Embedding Process

3.3.1 *ROI watermark embedding process*

(1) Initially, the ROI decomposes into two-levels using DWT to obtain the low-frequency and high-frequency components. The size of the low-frequency component is 1/4 of the ROI. The watermark is embedded into low frequency significant coefficients.

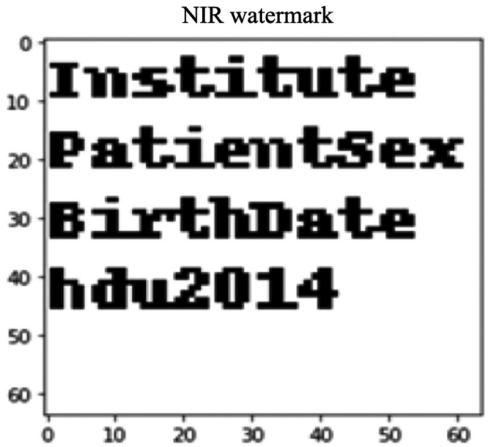

Fig. 3 NIR watermark.

(2) To embed the watermark information into the strong low frequency component, the quantization is calculated. In the quantized image, whereever the complex textural regions are present, the embedding strength is strong, and in the remaining smooth regions, the watermark embedding strength is weak. The quantization equation is shown as

$$q = c \times \ln \frac{|LH + HL + HH|}{2}, \tag{7}$$

where c is the quantization value with a value of 8 for this work; LH, HL, and HH are high frequency components; and q is the quantization step.

(3) The low-frequency components are quantified using the q value, which is defined as

$$O_q = \left[\frac{LL}{q}\right], \tag{8}$$

where LL is the low-frequency component.

(4) Next, watermarking image/information is encrypted using the logistic map(S):

$$S = X_{n+1} = \mu X_n (1 - X_n)$$
$$WM\_S\_\text{ROI} = WM\_\text{ROI} \oplus S,$$

where the $WM_S_$ROI is the encrypted watermark information, the X_n value is 0.9, and the μ value is 3.95.

(5) Finally, the encrypted watermark information is embedded on the low-frequency component using as

$$LL' = \begin{cases} O_q \times q & \text{if } \text{mod}(O_q, 2) = WM\_S\_\text{ROI} \\ O_q \times q + q & \text{if } \text{mod}(O_q, 2) \neq WM\_S\_\text{ROI} \end{cases}, \tag{9}$$

where LL' is a modified low-frequency component.

After embedding, the modified low-frequency and unmodified high-frequency components are combined. Then, the inverse DWT is applied for reconstructing the watermarked ROI. The watermark embedding diagram is shown in Fig. 4.

3.3.2 *NIR watermark embedding process*

(1) Initially, the NIR is divided into 8×8 blocks, then the DCT transform is applied to each block, and the low frequency band, middle frequency band, and high frequency band are obtained.

(2) Next, using zigzag sequence coefficients, the value of each block is sorted. After arranging the coefficient values in the middle frequency component, the watermark information is embedded.

(3) Before embedding, quantization is applied on the middle frequency coefficients, and it is shown in the following equation:

$$X_q = \text{round}(M_{\text{dct}}/q),$$

where q is the quantification step with a value of 4, X_q is the quantified middle frequency component, and M_{dct} is the original middle frequency component.

(4) Next, the original watermarking information is scrambled using the Arnold transform to improve security. Then, on each 8×8 block, the watermark embedding is calculated as

$$M'_{\text{dct}} = \begin{cases} (X_q - 1/2) \times q & \text{if } \text{mod}(X_q + WM\_A\_\text{NIR}, 2) = 1 \\ (X_q + 1/2) \times q & \text{if } \text{mod}(X_q + WM\_A\_\text{NIR}, 2) = 0 \end{cases}, \tag{10}$$

where M'_{dct} is the replaced middle frequency component, $WM_A_$NIR is the scrambled watermark information.

(5) Finally, inverse DCT transform is applied to reconstruct watermarked NIR.

The watermark embedding diagram is shown in Fig. 4.

Fig. 4 Embedding architecture diagram.

3.4 Extraction Process

3.4.1 *ROI watermark extraction*

(1) For extraction, the embedded medical image is separated into the ROI and NIR. Next, ROI is decomposed using DWT into two levels and then obtained the low-frequency component.

(2) Next, the quantization is calculated as

$$Z'_Q = \text{round}(LL'/q).$$

(3) After quantization extraction of the watermark is done, the extraction of the watermarking equation is calculated as

$$WM\_S\_\text{ROI}' = \text{mod}(Z'_Q, 2), \tag{11}$$

where WM_S_ROI' is the extracted watermark image.

(4) From the original watermarking image W'_{ROI} is got by performing XOR operation to extracted watermarking image WM_S_ROI' and 2-D matrix S:

$$W'_{\text{ROI}} = WM\_S\_\text{ROI}' \oplus S. \tag{12}$$

3.4.2 *NIR watermark extraction*

(1) The watermarked NIR is partitioned into non-overlapping 8×8 blocks, and DCT transform is applied on each block.

(2) Then, the coefficients of each block are sorted with the use of the zigzag sequence and a one-dimensional row vector is obtained. The mid-frequency coefficients from 13 to 19 are elected.

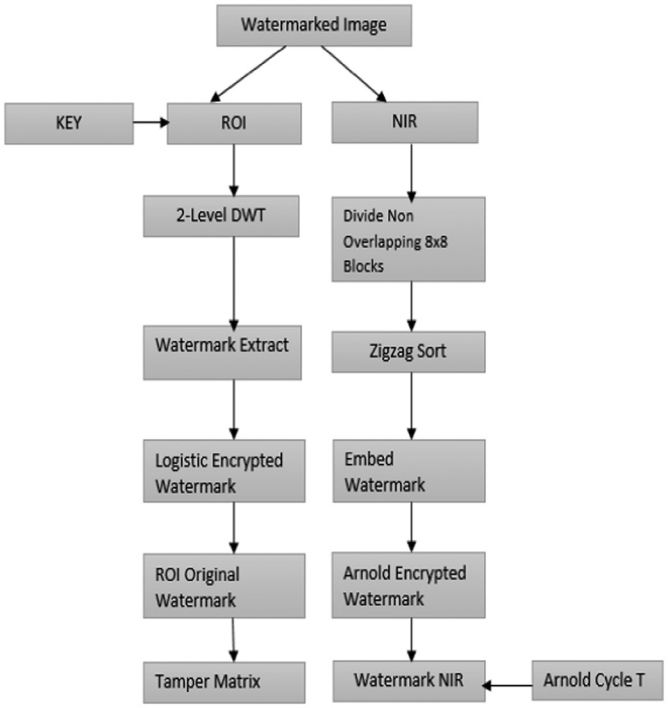

Fig. 5 Extracting process architecture diagram.

(3) Then, the coefficients are quantized using the quantization equation:

$$Z'_q = \text{floor}(M'_{\text{dct}}, 2). \tag{13}$$

(4) The watermark extraction of the NIR region is given as

$$WM\_A\_\text{NIR}' = \text{mod}(\text{Z}'_q, 2). \tag{14}$$

The complete process of extraction is shown in Fig. 5.

4 Experimental Results and Discussion

The experimental results of the proposed method on the typical dataset and its performance analysis are discussed in this section.

4.1 Input Images

The input images are collected from the Kaggle public databases, and images from the Indian scan center, in Madurai, India, are used for the testing purpose. These images are obtained from the human organ at different modalities. For the experiments purpose, 15 images are used. These images are identified as 1, 2, 3,...,15, with the size of each image being 512×512.

4.2 Evaluation Measures

The following measures are helpful for evaluating the performance of the system both subjectively and objectively.

4.2.1 *Peak signal to noise ratio*

$$\text{MSE} = 1/pr \sum_{i=0}^{p-1} \sum_{j=0}^{r-1} [M(i,j) - N(i,j)]^2, \tag{15}$$

$$\text{PSNR} = 10 \log_{10}(\text{MAX}^2/\text{MSE}), \tag{16}$$

where p and r are the height and width of the image, respectively. $M\ (i,j)$ and $N\ (i,j)$ are the input and watermarked images, respectively. MAX is the maximum value in an image.[12,13]

4.2.2 *Structural similarity*

The structural similarity (SSIM) is used to determine the similarity between the two images, and it is formulated as[14,15]

$$\mathrm{SSIM} = \frac{((2\mu_I\mu_W + C_1) * (2\sigma_{IW} + C_2))}{((\mu_I^2 + \mu_W^2 + C_1) * (\sigma_I^2 + \sigma_W^2 + C_2))}, \tag{17}$$

where μ_I and μ_W are the average of the input and watermarked images, respectively, and σ_I^2 and σ_W^2 are the variance of input and watermarked images, respectively. The value of SSIM ranges from -1 to 1, and when the two images are identical, the value is 1.

4.3 Robustness Analysis Against Attacks

To find the robustness of the method, two noisy attacks are applied on the watermarked images: salt and pepper noise and Gaussian noise (GN).

4.3.1 *Salt and pepper noise*

Salt and pepper noise is an impulse noise that is caused by a sharp and sudden disturbance in the image. The degraded pixels are fixed to be a minimum (0) or a maximum (1).[16,17]

4.3.2 *Gaussian noise*

The value of the Gaussian noise can be calculated using the Gaussian-distributed function. A GN attack can increase the perceptual visibility. However, it removes the edge information.

4.4 Experimental Discussion

4.4.1 *Results of ROI and NIR extraction*

In Fig. 6, the images represent the extraction of the ROI from the given input image and the image after cropping the ROI and NIR.

4.4.2 *Results of embedding and extraction of ROI*

The subjective result of ROI embedding is shown step by step in Fig. 7. In Fig. 7, Fig. 7(a) shows the original ROI extracted image, Fig. 7(b) shows the ROI encrypted image, Fig. 7(c) shows the quantized image, Fig. 7(d) shows the watermark embedded image, and Fig. 7(e) shows the embedded ROI image.

Figure 8 shows the watermark extraction process in which Fig. 8(a) shows the watermark embedded ROI image and Fig. 8(b) shows the watermark extracted from the ROI image.

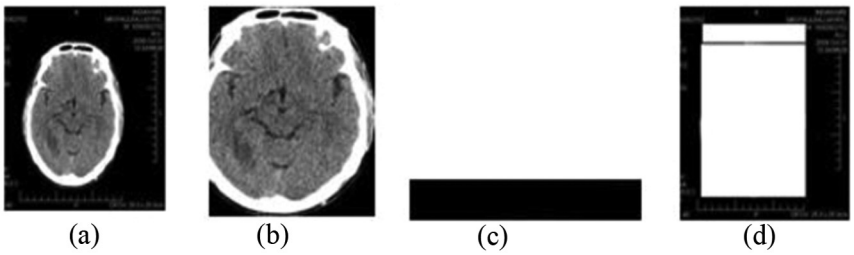

Fig. 6 Sample extraction of ROI watermark embedding: (a) input image, (b) ROI extraction, (c) NIR extraction, and (d) image after cropping the ROI and NIR.

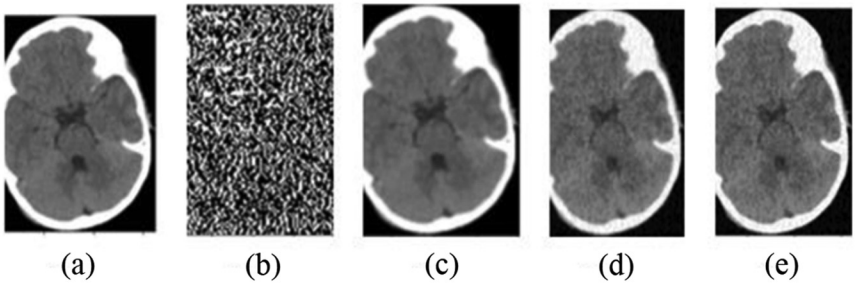

Fig. 7 Sample ROI watermark embedding process: (a) input ROI extracted image, (b) ROI encrypted image, (c) quantized on LL2 component image, (d) embedded on LL2 component image, and (e) embedded ROI image.

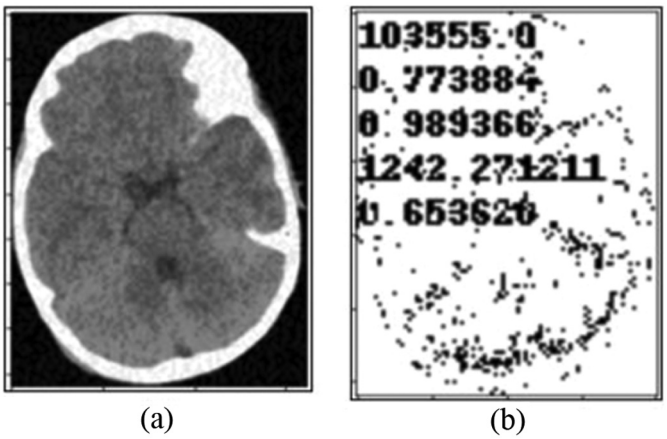

Fig. 8 Sample ROI watermark extraction process: (a) watermark embedded ROI image and (b) watermark extracted image.

4.4.3 *Results of embedding and extraction of NIR*

Figures 9 and 10 show the step by step embedding and extraction process on the NIR image.

4.4.4 *Robustness analysis against common noise attacks*

Figures 11 and 12 show the watermark extraction process on the watermarked image with added noise. From Figs. 11 and 12, it is observed that the proposed method can extract the watermark image from the noisy attack without disturbance.

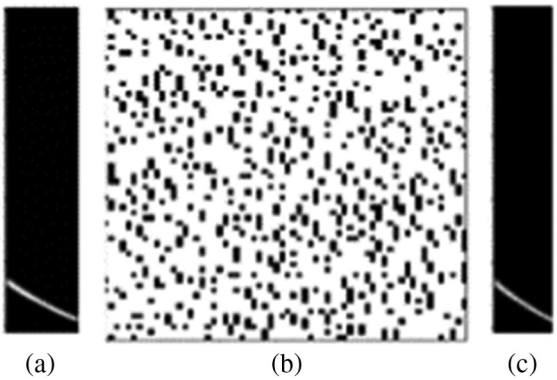

Fig. 9 Sample NIR watermark embedding process: (a) input NIR image, (b) NIR encrypted image, and (c) embedded NIR image.

(a) (b) (c)

Fig. 10 Sample NIR watermark extraction process: (a) input embedded NIR image, (b) extracted NIR encrypted watermark image, and (c) decrypted NIR watermark image.

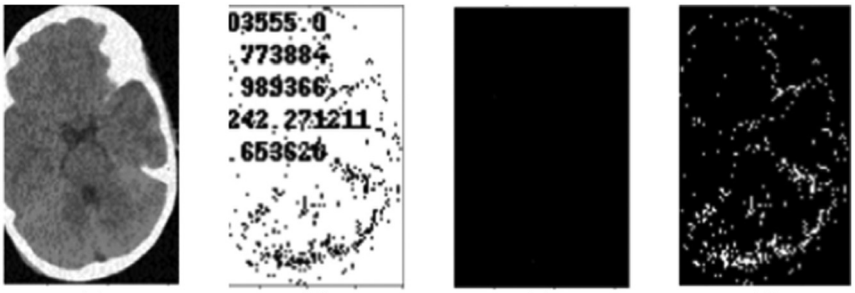

(a) (b) (c) (d)

Fig. 11 Sample testing watermarked image against SPN: (a) added SPN to watermarked image, (b) extracted watermark from (a), (c) watermarked image error map, and (d) watermark error map.

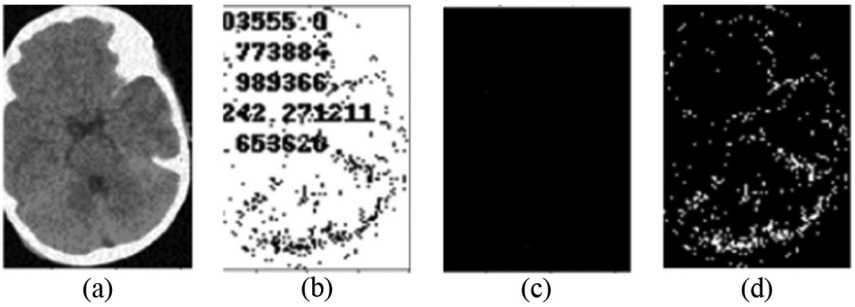

(a) (b) (c) (d)

Fig. 12 Sample testing watermarked image against GN: (a) added GN to watermarked image, (b) extracted watermark from (a), (c) watermarked image error map, and (d) watermark error map.

4.4.5 *Performance analysis*

Table 2 presents the performance comparison of different images against various attacks with the mean square error (MSE), peak signal-to-noise ratio (PSNR), and SSIM measures. From Table 2, it is observed that the MSE, PSNR, and SSIM values range from 0.0513 to 0.0630, 41.0211 to 45.7621, and 0.9650 to 0.9999 against no attack, salt and pepper noise (SPN), and GN, respectively.

In addition, the proposed method is compared with the existing techniques using PSNR, MSE, and SSIM measures for robust analysis, which is presented in Table 3. Further, the time complexity of the embedding process is $O(n^2)$ and that of the extraction process is $O(n^2)$.

5 Conclusion

In this paper, we have implemented a multiple watermark scheme based on quantized DWT-DCT embedding. In addition, implemented attack vectors, such as SPN and GN, are used to show the

Table 2 Performance comparison of different images against various attacks using MSE, PSNR, and SSIM measures.

Image sequence number	Noisy name	MSE	PSNR	SSIM
1	No attack	0.0523	45.7621	0.9999
2		0.0520	43.2532	0.9983
3		0.0525	42.5545	0.9948
4		0.0513	43.8467	0.9923
5		0.0532	45.4021	0.9945
6		0.0521	45.0745	0.9915
7		0.0524	45.2701	0.9952
8		0.0512	45.6712	0.9991
9		0.0520	43.1551	0.9974
10		0.0541	42.4545	0.9954
11		0.0532	43.4678	0.9981
12		0.0535	45.0412	0.9967
13		0.0564	45.7051	0.9914
14		0.0531	45.4215	0.9945
15		0.0560	45.6123	0.9986
1	SPN	0.0563	45.1634	0.9794
2		0.0560	43.0501	0.9761
3		0.0565	42.0112	0.9726
4		0.0553	43.0231	0.9701
5		0.0572	44.2321	0.9733
6		0.0571	44.1725	0.9754
7		0.0574	44.9711	0.9731
8		0.0562	45.2121	0.9750
9		0.0570	42.5124	0.9711
10		0.0591	41.4521	0.9732
11		0.0582	42.6746	0.9740
12		0.0585	43.4124	0.9723
13		0.0601	44.7521	0.9703
14		0.0581	44.1225	0.9734
15		0.0599	44.1312	0.9745

Table 2 (*Continued*).

Image sequence number	Noisy name	MSE	PSNR	SSIM
1	GN	0.0583	44.9621	0.9736
2		0.0580	42.9813	0.9710
3		0.0585	41.9921	0.9661
4		0.0573	42.9418	0.9656
5		0.0592	44.0021	0.9693
6		0.0591	43.9756	0.9701
7		0.0594	44.5734	0.9689
8		0.0582	45.9994	0.9701
9		0.0590	42.1212	0.9685
10		0.0611	41.0211	0.9621
11		0.0602	42.3214	0.9680
12		0.0605	43.0213	0.9682
13		0.0621	44.2115	0.9653
14		0.0601	43.9921	0.9674
15		0.0629	43.8773	0.9687

Table 3 Performance comparison with existing watermarking techniques using PSNR, MSE, and SSIM measures for robustness analysis.

Methods	Noisy name	PSNR	MSE	SSIM
Soualmi et al.[18]	No attack	44.30	—	0.9987
	Salt and pepper	—	—	0.8022
	Gaussian		—	—
Giakoumaki et al.[19]	No attack	43.23	—	
	Salt and pepper	—	—	—
	Gaussian	—	—	—
Moniruzzaman et al.[20]	No attack	44.03	2.57	—
	Salt and pepper	—	—	—
	Gaussian	—	—	—
Proposed	No attack	45.76	0.0512	0.9999
	Salt and pepper	45.21	0.0553	0.9794
	Gaussian	45.99	0.0582	0.9736

robustness of the DWT-DCT embedding process using quality metrics. The proposed DWT-DCT watermarking obtained better results than the existing method. In the future, the proposed method could be optimized and improved through more effort and higher knowledge of the domain, which will enable multiple data types to be hidden in medical images and further improve security in the electronic medical record field.

Disclosures

The authors of this research article declare no conflicts of interest in preparing this research article.

Code and Data Availability

The code and data presented in this article are publicly available in https://github.com/AryakRoy/DWT-DCT-Watermark-Algorithm.

References

1. J. Lu et al., "Multiple watermark scheme based on DWT-DCT quantization for medical images," *J. Inf. Hiding Multimedia Signal Process.* **6**(3), 458–472 (2015).
2. G. Singh, "A review of secure medical image watermarking," in *IEEE Int. Conf. Power, Control, Signals, and Instrum. Eng. (ICPCSI)*, IEEE, pp. 3105–3109 (2017).
3. S. Sun and R. Zhang, "Region of interest extraction of medical image based on improved region growing algorithm," in *Int. Conf. Mater. Sci., Energy and Environ. Eng. (MSEEE)*, IEEE, pp. 360–364 (2017).
4. P. S. Nayak et al., "Reliable transmission and storage of medical images with patient information using error control codes," in *Proc. IEEE INDICON*, pp. 147–150 (2004).
5. H. Trichili, M.S. Bouhlel, and B. Solaiman, "A new image watermarking scheme for medical image archiving," in *Inf. and Commun. Technol. (ICTTA06)*, pp. 1498–1503 (2006).
6. J. M. Zain and M. Clarke, "Reversible region of non-interest (RONI) watermarking for authentication of DICOM images," *Int. J. Comput. Sci. Network Secur.* **7**, 19–28 (2011).
7. O. M. Al-Qershi and B. E. Khoo, "Authentication and data hiding using a hybrid ROI based watermarking scheme for DICOM images," *J. Digital Imaging* **24**, 114–125 (2011).
8. A. K. Salwa et al., "Wavelet packets-based blind watermarking for medical image management," *Open Biomed. Eng. J.* **4**, 93–98 (2010).
9. S. Natu, P. Natu, and T. Sarode, "Improved robust digital image watermarking with SVD and hybrid transform," in *Int. Conf. Intell. Commun. and Comput. Tech. (ICCT)*, IEEE, pp. 177–181 (2017).
10. I. Assini et al., "A robust hybrid watermarking technique for securing medical image," *Int. J. Intell. Eng. Syst.* **11**(3), 169–176 (2018).
11. M. Begum and M. S. Uddin, "Analysis of digital image watermarking techniques through hybrid methods," *Adv. Multimedia* **2020**, 7912690 (2020).
12. S. Rajkumar and S. Kavitha, "Redundancy discrete wavelet transform and contourlet transform for multimodality medical image fusion with quantitative analysis," in *3rd Int. Conf. Emerg. Trends in Eng. and Technol.*, IEEE, pp. 134–139 (2010).
13. A. Pillai et al., "Adaptive new top-hat transform and multi-scale sequential toggle operator based infrared image enhancement," in *Innov. in Power and Adv. Comput. Technol. (i-PACT)*, IEEE, pp. 1–5 (2017).
14. S. Satapathy, K. Jalan, and R. Soundrapandiyan, "Discrete wavelet transform based invisible watermarking scheme for digital images," in *Smart Intelligent Computing and Applications*, S. C. Satapathy, V. Bhateja, and S. Das, Eds., pp. 207–215, Springer, Singapore (2019).
15. R. Soundrapandiyan and P. C. Mouli, "Robust pedestrian detection in infrared images using rotation and scale invariant-based structure element descriptor," *Int. J. Signal Imaging Syst. Eng.* **10**(3), 157–167 (2017).
16. R. Soundrapandiyan et al., "An efficient DWT and intuitionistic fuzzy based multimodality medical image fusion," *Int. J. Imaging Syst. Technol.* **27**(2), 118–132 (2017).
17. S. Kumar and R. Soundrapandiyan, "A multi-image hiding technique in dilated video regions based on cooperative game-theoretic approach," *J. King Saud Univ.-Comput. Inf. Sci.* **34**, 5841–5855 (2021).
18. A. Soualmi, A. Alti, and L. Laouamer, "A new blind medical image watermarking based on weber descriptors and Arnold chaotic map," *Arab. J. Sci. Eng.* **43**, 7893–7905 (2018).
19. A. Giakoumaki, S. Pavlopoulos, and D. Koutsouris, "Multiple digital watermarking applied to medical imaging," in *IEEE Eng. in Med. and Biol. 27th Annu. Conf.*, IEEE, pp. 3444–3447 (2006).
20. M. Moniruzzaman, M. A. K. Hawlader, and M. F. Hossain, "Wavelet based watermarking approach of hiding patient information in medical image for medical image authentication," in *17th Int. Conf. Comput. and Inf. Technol. (ICCIT)*, IEEE, pp. 374–378 (2014).

Rajkumar Soundrapandiyan is currently working as an associate professor in the School of Computer Science and Engineering, Vellore Institute of Technology (VIT), Vellore, Tamil Nadu, India. He received his PhD from VIT, Vellore, India, in 2017. His research interests include computer vision, visual perception, object detection, medical image processing, infrared image processing, biometrics, information hiding, and network security.

Kannadasan Rajendiran is an associate professor in the School of Computing Science and Engineering at VIT, Vellore, India. He received his BE and ME degrees in computer science and engineering from Anna University and his PhD in computer science and engineering from VIT, Vellore. He has 15+ years of experience in teaching and he has published about 37 papers in international journals on machine learning, nature-inspired algorithms, healthcare, and bioinformatics. His research interest includes DNA computing, theoretical computing and bioinformatics, compiler design, digital logic design.

Arunkumar Gurunathan is currently working as an associate professor in the School of Computer Science and Engineering, VIT, Tamil Nadu, India. He received his BE degree in computer science and engineering from Madras University, Chennai, India, in 2001, his MTech degree in computer science and engineering from VIT University, Vellore, India, in 2007. He received his PhD from VIT, Vellore, India, in 2018. His research interest includes autonomic computing, web services, cloud computing, big data, artificial intelligence, and machine learning. He has published more than 15 research papers in reputed international conferences and journals.

Akila Victor is currently working as an associate professor in the School of Computer Science and Engineering in VIT, Vellore. She received her PhD from VIT University, Vellore, India, in 2018. Her research interest includes image processing, computer vision, medical image processing, and machine learning. She has published more than 20 research papers in reputed international journals and book chapters. She is a life member of CSI.

Ramani Selvanambi is an associate professor in the School of Computing Science and Engineering at VIT, Vellore, India. He received his BE degree in computer science and engineering from Madras University and his MTech degree in computer science and engineering from Bharathidasan University and his PhD in computer science and engineering from VIT, Vellore. He has 14+ years of experience in teaching and 2 years of experience in the consultancy and software industry. He has published about 45 research papers in international journals on machine learning in healthcare, nature-inspired algorithms, cyber security. His research interest includes data mining, machine learning, database systems, optimization techniques, and cyber security. He is a senior member in an IEEE, professional member in ACM, a life member in CSI, and member in other technical societies.